JOURNAL OF MATERIALS SCIENCE 21 (1986) 3194–3210

Modulus-maps for amorphous polymers

D. G. GILBERT
BP Research Centre, Chertsey Road, Sunbury-on-Thames, Middlesex TW16 7LN, UK
M. F. ASHBY, P. W. R. BEAUMONT
Engineering Department, Cambridge University, Trumpington Street, Cambridge CB2 1PZ, UK

This paper explores the possibility of constructing modulus-mechanism maps for amorphous polymers. Four regimes are identified: the glassy regime, the visco-elastic regime, the rubbery regime and the regime of viscous flow (melting), truncated by decomposition. Constitutive laws for each regime are assembled and adapted to give a good description of a large body of experimental data for amorphous polymethylmethacrylate and polystyrene. The adjusted laws are then used to construct diagrams which relate the time and temperature-dependent modulus, $E(t, T)$, to the temperature and the loading time (or frequency). The diagrams are divided into fields corresponding to the four regimes. A diagram summarizes the small-strain mechanical behaviour of the polymer over a wide range of conditions.

Nomenclature

T	Temperature (K).
σ	Tensile or compressive stress (MPa).
ε	Tensile or compressive strain.
$\dot{\varepsilon}$	Tensile or compressive strain rate (sec^{-1}).
t	Time (sec).
ν	Frequency (sec^{-1}).
E	Time and temperature dependent Young's modulus (GPa).
E_0	Modulus of 0 K (GPa).
α_m	Temperature coefficient of modulus.
T_g	Glass temperature (K).
T_D	Depolymerization temperature (K).
$\bar{M}_w$, M_{cr}, $\bar{M}_e$	Molecular weights ($kg\,mol^{-1}$).
Q_m	Mean activation energy ($kJ\,mol^{-1}$).
$\Delta Q/Q_m$	Fractional standard deviation of activation energy.
$\Delta E/E_0$	Fractional modulus drop at a transition.
a_T	Shift factor for time–temperature equivalence.
η	Viscosity ($Nsec\,m^{-2}$).
η_0	Pre-exponential for viscosity ($Nsec\,m^{-2}$).
α_g, α_v	Bulk thermal expansion coefficient below and above T_g (K^{-1}).
C_1, C_2	WLF constants (–, K).
ϱ	Density ($kg\,m^{-3}$).
f_v	Fractional free volume.
$V(\varepsilon)$	Internal energy per unit volume ($J\,m^{-3}$).
R	Gas constant ($8.314\,J\,mol^{-1}\,K^{-1}$).
v_0	A pre-exponential frequency factor (sec^{-1}).

1. Introduction

When a polymer is loaded, it suffers deformation which, in general, increases with time of loading. For uniaxial loading, the resistance to small-strain deformation is conventionally measured by the *time and temperature dependent modulus*, $E(t, T)$ (from now on simply called E). If, for instance, a constant stress σ is applied to a sample of the polymer, giving a strain $\varepsilon(t, T)$ after a time t at temperature T, then

$$E = \frac{\sigma}{\varepsilon(t, T)} \quad (1)$$

Linear amorphous polymers like polymethylmethacrylate (PMMA) or polystryene (PS) show four distinct regimes of deformation, in each of which the modulus has certain characteristics, illustrated in Fig. 1.

(a) The glassy regime, with a modulus of between 1 and 10 GPa, associated with stretching and bending of intermolecular bonds, and showing only a slight time-dependence associated with a number of secondary relaxations.

(b) The glass-transition regime, in which the modulus drops steeply from around 1 GPa to near 1 MPa with increasing temperature or time of loading.

(c) The rubbery regime, with a modulus around 1 MPa, associated with the rubber-like sliding of the long-chain network of molecules, constrained by entanglements which behave (physically) like cross-links.

(d) The viscous regime, at temperatures well above the glass transition temperature, in which the polymer can be thought of as a viscous liquid; its molecules move relative to each in a snake-like manner (reptation) which, when biased by stress, leads to viscous flow.

(e) A regime of decomposition in which chemical breakdown begins and the mechanical properties change in an uncontrolled way.

0022–2461/86 $03.00 + .12

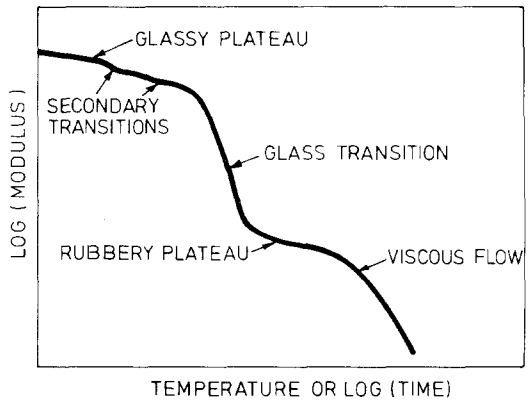

Figure 1 Schematic illustration showing the regimes of behaviour typical of an amorphous polymer.

Each regime has been studied and modelled in more or less detail, and constitutive relations for each have been formulated (they are reviewed below). Experimental data for E are available for PMMA and PS.

Our aim, simply put, is to construct a quantitatively accurate version of Fig. 1. To do so, we fit the constitutive relations to the data (requiring some modification to the models) and examine how they can be combined to give a self-consistent description of small-strain deformation from 0 K to above the melting temperature, and for all practical loading times. The results are assembled into diagrams (one form of which resembles Fig. 1) which summarize the small-strain deformation behaviour of each polymer as a function of temperature, time and frequency.

We now examine the four regimes in more detail, reviewing and selecting among the constitutive laws for each. Symbols and their definitions are listed in the nomenclature.

2. Deformation mechanisms

2.1. The Glassy regime and the β, γ and δ relaxations

The glass temperature, T_g, roughly divides the low temperature behaviour from the high. Well below T_g, linear amorphous polymers have Young's moduli of, very roughly, 3 GPa. In this regime, bond stretching and bending controls the modulus which directly reflects the stiffness of the Van der Waals bonds which bind one chain to another. They are shown as dotted lines in Fig. 2. The covalent C–C bonds which form the chain backbone (full lines) are about 100 times stiffer than the Van der Waals bonds, and their stretching and bending contributes nothing significant to the elastic deformation. Rotation about a C–C bond is possible. The single C–C bond rotates easily; steric hindrance, and thus the Van der Waals bonds, again, limit its extent [1–4].

If the internal energy of the polymer, per unit volume, is $V(\varepsilon)$, then the glassy modulus at 0 K is calculated (in principle) by forming the second derivative of $V(\varepsilon)$ with respect to ε

$$E = -\frac{d^2V(\varepsilon)}{d\varepsilon^2} \qquad (2)$$

But the fundamental understanding of intermolecular bonding in polymers is still too poor to

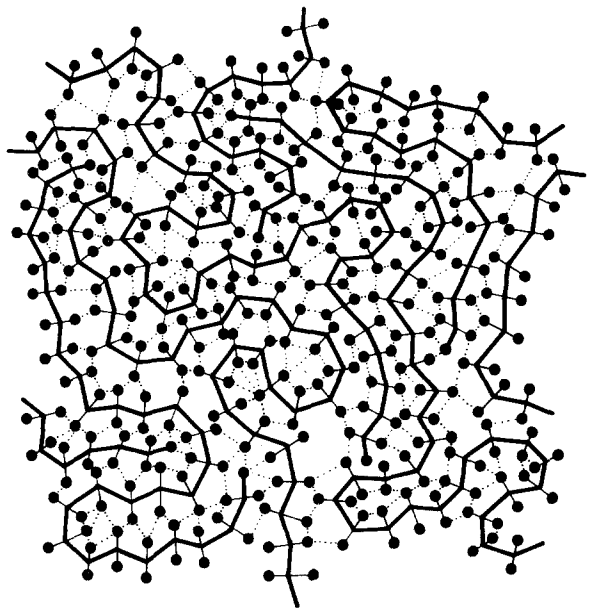

Figure 2 Schematic illustration of a linear amorphous polymer. The covalently-linked chains (full lines) are bonded to each other by weak Van der Waals forces (dotted lines) which determine the glassy modulus.

allow $V(\varepsilon)$ to be computed accurately from first principles (in practice, experimental data for E are used to calibrate the potential functions, rather than the other way round). Instead, the modulus at absolute zero, E_0, is obtained by extrapolating experimental measurements of E at slightly higher temperatures to absolute zero. Values of E_0 obtained in this way are listed, together with other material data, in Table I.

Increasing the temperature has two distinct effects. First, thermal expansion increases the molecular separation and lowers the Van der Waals restoring forces: this gives a slow drop in modulus, but does not introduce a time or frequency-dependence. Second, the thermal energy of the molecules permits thermally-activated local rearrangements (usually, rotations about a C–C bond), giving time-dependent strain and an additional drop in modulus.

The first effect leads to a roughly linear decrease in modulus with increasing temperature. Yannas and Luise [3] developed this idea: thermal expansion increases the interchain distance, reducing the force required for intermolecular deformation by bond stretching. The final form of their equation is cumbersome but simplifies to a linear relationship at low temperatures which can be written:

$$E = E_0\left(1 - \alpha_m \frac{T}{T_g}\right) \qquad (3)$$

We use this to describe the drop in modulus caused by thermal expansion. The dimensionless coefficients α_m which best described the low temperature data for each polymer are listed in Table I.

The second contribution comes from the small thermally-activated rearrangements of side groups or of short segments of chain at "loose sites" in the amorphous structure (Fig. 3). These relaxation processes, all occurring at temperatures below T_g (and known, in order of decreasing temperature, as the β, γ and δ relaxations) give additional strain, and they thereby

TABLE I Material data used to construct the diagrams

Material	PMMA		PS	
Thermal and structural data				
Glass temperature, T_g (K)	378		373	
Bulk coefficient of T-expansion below T_g, α_g (K^{-1})	2.69×10^{-4}		2.27×10^{-4}	
Bulk coefficient of T-expansion above T_g, α_v (K^{-1})	6.25×10^{-4}		6.12×10^{-4}	
Mean molecular weight, $\bar{M}_w$ (kg mol^{-1})	10^2		10^2	
Modulus data				
Young's modulus at 0 K, E_0 (GPa)	8.6		6.2	
T-coefficient of modulus, α_m	0.28		0.3	
Data for β, γ and δ relaxation				
Mean activation energy, Q_m (kJ mol^{-1})	γ	β	δ	β
Fractional spread of activation energy, $\Delta Q/Q_m$	13	121.3	9.4	125
Modulus drop, $\Delta E/E_0$	0.20	0.20	0.4	0.4
Position of peak, T^*/T_g	0.07	0.47	0.29	0.03
Pre-exponential, η_0 (Nsec m^{-2})	0.26	0.75	0.10	0.80
	15.8	1.5×10^{-15}	3.5×10^{-6}	8.3×10^{-17}
Data for glass transition				
Constant C_1 of WLF equation	17.4		17.4	
Constant C_2 of WLF equation for $T < T_g$ (K)	143		143	
Constant C_2 of WLF equation for $T > T_g$ (K)	52		52	
Fractional spread of $C_1(\phi = \Delta C_1/C_1)$	0.05		0.08	
Data for rubbery plateau				
Molecular weight between entanglements, $\bar{M}_e$ (kg mol^{-1})	9.15		14.0	
Density at $T = T_g$, $\varrho(T_g)$ (kg mol^{-3})	1.16×10^3		1.03×10^3	
Data for viscous flow				
Critical molecular weight, M_{cr} (kg mol^{-1})	30		35	
Pre-exponential, η_0 (Nsec m^{-2})	1.1×10^{16}		2×10^{15}	
Fractional spread of $C_1(\phi = \Delta C_1/C_1)$	0.11		0.05	
Data for decomposition				
Depolymerization temperature, T_d/T_g	1.44		1.46	

reduce the modulus a little. Each relaxation is positioned (for a given loading time or frequency) at a characteristic temperature at which thermal energy becomes sufficient to activate the rearrangement.

Like similar relaxations in crystalline solids, the response of the material to load is conveniently described by a rheological model. The simplest that is of any real use is the standard linear solid (Fig. 4a), composed of two springs of modulus E and ΔE, and a dashpot of viscosity:

$$\eta = \eta_0 \exp\left(\frac{Q}{RT}\right) \quad (4)$$

where Q is the activation energy for the process, R the gas constant and η_0 a constant which is chosen to fix the position of the drop in modulus. The standard-linear model gives a good phenomenological description of most anelastic relaxations in crystals, and relaxations in glasses do, very roughly, have the same characteristics. But more careful examination of data for amorphous polymers shows that the standard linear solid is too simple. Its response leads to an almost step-like drop in modulus at the characteristic temperature; the real relaxation is broader (Fig. 5). This is no surprise. In PMMA, for instance, the β-relaxation is thought to be caused by a motion of the ester side-group, the γ-relaxation by the motion of one of the two methyl groups and the δ-relaxation by the motion of the other one (Fig. 3). The amorphous chain-packing grips of some of these more tightly than others, so that each relaxation has a spectrum of activation energies. The response is then more realistically described by the parallel coupling of "springs and dashpot" units shown in Fig. 4b, each dashpot describing a part of the activation energy spectrum.

This arrangement of units, rather than a more

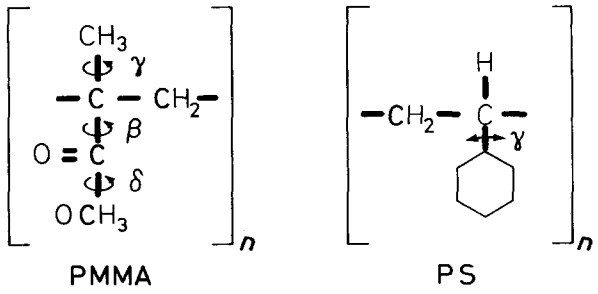

Figure 3 Schematic illustration of the secondary relaxations in PMMA and PS.

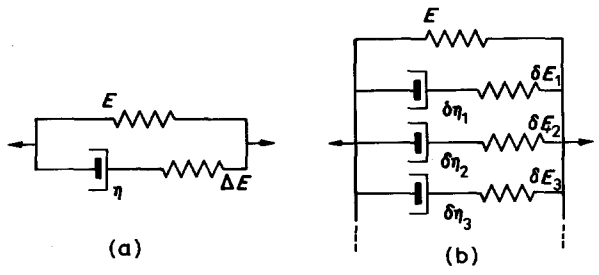

Figure 4 (a) The standard linear solid, (b) the extended model. If a Gaussian distribution of relaxation times is assumed, the model requires only one more parameter than the standard-linear solid to describe it completely.

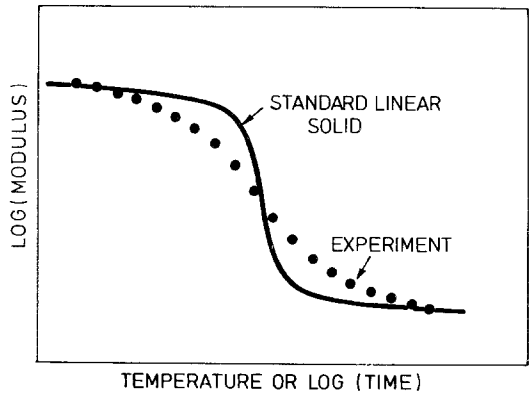

Figure 5 The response of the standard-linear solid with a single activation energy compared with experiment.

general one involving units in series and parallel, is justified in the following way. Relaxation involves the motion of isolated side groups — those which, at a given instant, are less tightly gripped than the rest. Each can be thought of as a small spherical volume in which viscous deformation takes place, embedded in an elastic matrix. The constitutive equation for a material consisting of viscous inclusions in an elastic matrix is discussed by Brown [5]: provided the dispersion of viscous spheres is *dilute* (meaning that they are well separated), the material behaves like a standard linear solid (as in Fig. 4a). If each of the spherical volumes has a different activation energy (as in the case for the side-group relaxations discussed here) the same reasoning leads to the conclusions that the material behaves in a way described by Maxwell elements in parallel, as in Fig. 4b.

As explained, the distribution of activation energies arises from differences in local packing density which make it harder to move some side-groups than others. We have used a Gaussian distribution of activation energies with a mean Q_m and a standard deviation ΔQ. The proportion of units (that is, the fraction of the spheres which relax) with activation energies between Q and δQ is $f(Q)\,\delta Q$ where

$$f(Q) = \frac{1}{(2\pi)^{1/2}\Delta Q}\left[\exp -\frac{1}{2}\left(\frac{Q - Q_m}{\Delta Q}\right)^2\right] \quad (5)$$

This defines a weighting function for each unit (Fig. 6) so that the modulus drop δE_i associated with full relaxation of the ith unit is

$$\delta E_i = \Delta E f(Q)\delta Q \quad (6)$$

where ΔE is the total modulus drop associated with the relaxation. This method introduces only one new variable, the standard deviation, ΔQ, into the calculation of the relaxation; it is chosen so that the width of the relaxation (Fig. 5) matches experiment. Data for ΔE, Q_m and $\Delta Q/Q_m$ for PMMA and PS are listed in Table I.

2.2. The glass–rubber transition (the visco-elastic regime)

As the temperature is raised, the Van der Waals bonds start to melt. Then segments of the previously elastically-bonded chains slide relative to each other and the material behaves in a visco-elastic way. Within this regime it is found that the modulus E at one temperature can be related to that at another by a change in the time scale only, that is, there is an *equivalence between time and temperature*. This means that the curve describing the modulus at one temperature can be superimposed on that for another by a constant horizontal displacement log (a_T) along the log (t) or log (ν) axis, as shown in Fig. 7.

In crystalline solids (notably metals) the time–temperature equivalence for the rate of diffusion, for creep, and for other thermally activated processes, is well known; it follows from the kinetic theory of simple thermally activated processes. The diffusive jump frequency at one temperature, T_1 for example, is related to that at another temperature, T_2, by

$$\log\left(\frac{\nu_1}{\nu_2}\right) = \log a_T = \frac{Q}{2.3R}\left(\frac{1}{T_2} - \frac{1}{T_1}\right) \quad (7)$$

where Q is the activation energy for diffusion. A simple shift along the frequency or time axis by log (a_T) then brings the response at T_1 into coincidence with that at T_2.

A spectrum of activation energies (which is inevitable in an amorphous system) does not destroy the time–temperature equivalence though it may change its form. If the width of the spectrum, ΔQ, is small (so that $\Delta Q \gg RT$) then it is easily shown that the shift factor defined by Equation 7 still applies, and the relaxation follows simple Arrhenius kinetics. The β, γ

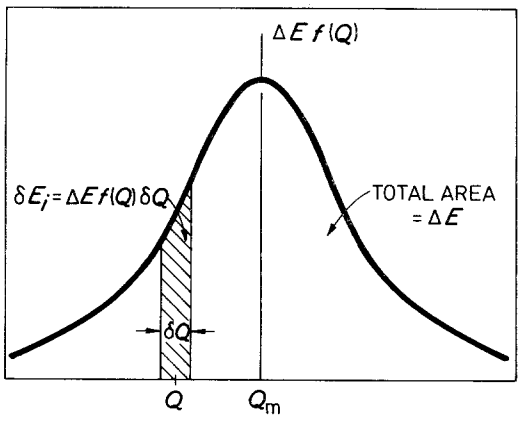

Figure 6 A Gaussian distribution for the fraction of units with activation energies between Q and $Q + \delta Q$ requires an associated distribution of moduli δE_i, illustrated here.

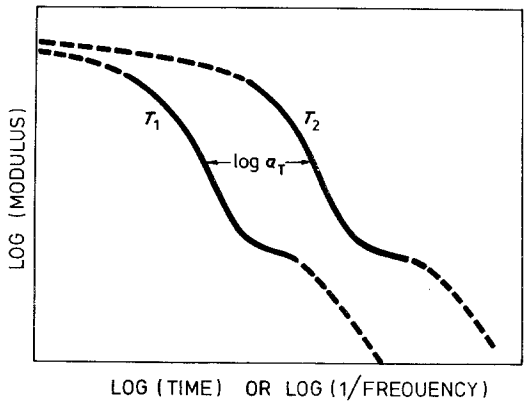

Figure 7 Schematic illustration of the time–temperature equivalence for the modulus.

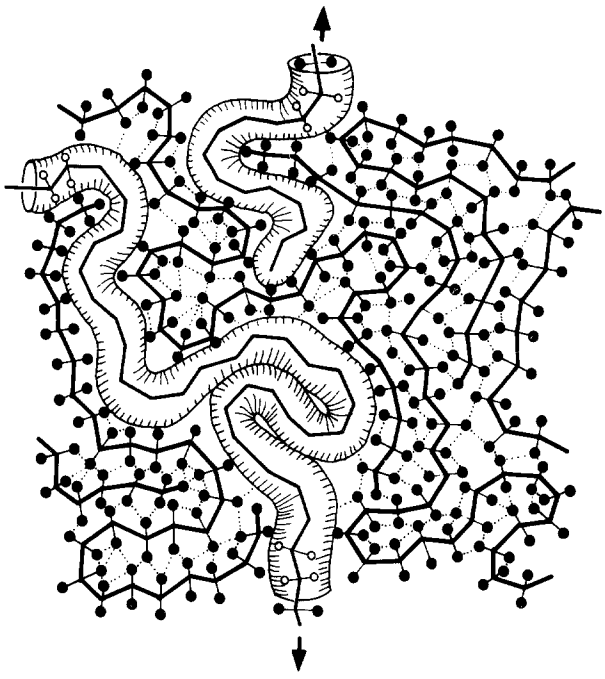

Figure 8 Schematic illustration of viscous diffusive motion, or reptation, of a polymer chain in the tube defined by its immediate surroundings.

and δ relaxations do, in fact, give linear Arrhenius plots; those for PMMA and PS are shown later. But the α, or glass–rubber transition is more complicated. Experiments on liquids and on amorphous polymers [6] are not well described by Equation 7; they suggest, instead, a shift factor (the "WLF" shift factor) given by

$$\log a_T = \frac{C_1(T - T_g)}{C_2 + T - T_g} \tag{8}$$

where C_1 and C_2 are constants (the "WLF" constants, with T_g as reference temperature). In the limit $T \gg C_2 - T_g$, this reduces to the simpler Equation (7) with $C_1 = Q/2.3RT_g$. But the values of C_2 are such that this is never a satisfactory approximation and a new, broader physical interpretation must be sought.

The quest had produced a number of models (for brief reviews, see [7–9]). From these the following simplified picture can be assembled. Viscous chain motion is caused by the stress-biased diffusion of polymer chains within the tubes which define their surroundings, as shown in Fig. 8. This snake-like diffusive motion, or "reptation", must involve the propagation of compression or shear wave pulses or kinks along the chain: in either case, the projecting side groups of one chain must move over and past those with which they mesh in the surrounding tube, as shown in Fig. 9.

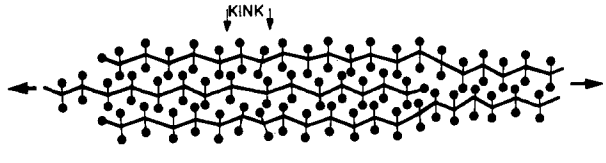

Figure 9 The diffusion of compressice kinks along a polymer chain, leading to relative motion of chains.

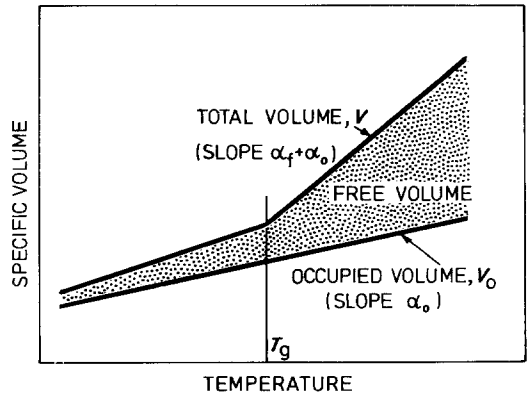

Figure 10 Typical variation of specific volume with temperature for an amorphous polymer.

The frequency of occurrence of the unit step associated with producing viscous strain depends, as in crystals, on the product of two probabilities: the probability p_1 that a unit segment of the polymer chain has enough thermal energy to jump over the energy barrier which separates it from an adjacent position; and the probability p_2 that this second site is "vacant", i.e. that it has sufficient unoccupied volume associated with it to accommodate the jumping segment. The first probability, p_1, is given by an Arrhenius law, as in a crystal. The second probability, p_2, is more complicated. In crystals, unoccupied or "free" volume is quantized as vacancies of fixed volume. Free volume exists in amorphous sytems too, but it is obviously not quantized in the way it is crystals. When the specific volume of an amorphous polymer is plotted against temperature (Fig. 10) there is a change of slope at T_g. The free volume [10, 11] is the difference between the total volume, V, and that occupied by the molecules themselves, V_0. The occupied volume is that of a dense (though disordered) packing of cylinders, one surrounding each chain, with a radius equal to the Van der Waals radius plus that associated with the local thermal vibrations of the atoms. What is left over is "free" in the sense that it can redistribute continuously. Instead of a thermal-equilibrium concentration of vacancies, each of fixed volume, which move around continuously, the free volume exists (in thermal equilibrium, of course) as a spectrum of void volumes which continuously open up and close again. The thermal expansion data show that (unlike crystals) the free volume increases linearly with temperature. Defining the fractional free volume as

$$f_v = \frac{V - V_0}{V} \tag{9}$$

we have that

$$f_v = f_g + \alpha_f(T - T_g) \tag{10}$$

where f_g is the fractional free volume at the glass temperature. The quantity α_f is the free-volume expansion coefficient: it is the difference between the total expansion coefficient and that for the occupied volume. The figure shows how the value of α_f changes at T_g; above T_g it is large, below it is much smaller (some authors take it to be zero, but a small finite value may

be more realistic). The probability, p_2, is then the chance that, adjacent to a jumping segment, a local free volume of f_c or greater is available (f_c is the fractional volume required to accommodate the jumping segment). This probability [12] is

$$p_2 = \exp - \left(\frac{Af_c}{f_v}\right) \tag{11}$$

Then the viscosity at temperature T, relative to that at T_g is given by $p_1(T)p_2(f)/(p_1(T_g)p_2(f_g)$, or

$$\frac{\eta(T)}{\eta(T_g)} = \exp\left[\frac{Q}{R}\left(\frac{1}{T} - \frac{1}{T_g}\right)\right] \exp\left[B\left(\frac{1}{f_v} - \frac{1}{f_g}\right)\right] \tag{12}$$

where $B = Af_c$. The apparent activation energy is given by

$$\frac{\partial \ln \eta(T)}{\partial 1/RT} = Q + \frac{BRT^2}{f^2}\alpha_f$$

where $\alpha_f = \partial f_v/\partial T$. Well below T_g the free volume is almost independent of temperature (Fig. 10); then the first term is dominant and we find Arrhenius behaviour (though with a spectrum of activation energies). At and above T_g, on the other hand, f_v increases rapidly with temperature; and it is probable that Q, correspondingly, decreases [13]. When Q is small, the second term becomes dominant. Experiments on viscous liquids support this view [14, 15] so that data are well described by

$$\frac{\eta(T)}{\eta(T_g)} = \exp\left[B\left(\frac{1}{f_v} - \frac{1}{f_g}\right)\right] \tag{13}$$

with the constant B close to unit. Substituting Equation 10 leads immediately to the WLF equation

$$\log a_T = \log \frac{\eta(T)}{\eta(T_g)} = \frac{-[(B/2.3f_g)(T - T_g)]}{(f_g/\alpha_f + T - T_g)} \tag{14}$$

with $C_1 = -B/2.3f_g$ and $C_2 = f_g/\alpha_f$. One of the many achievements of the work of Ferry and his co-workers [6, 16] is the demonstration that C_1 and C_2 are universal constants at and above T_g. The same constants describe polymers also, implying that f_g and α_f, too, are universal constants. It is helpful to note their magnitudes: taking $B = 1$, the fractional free volume at the glass temperature, f_g, is found to be 0.025; and the free-volume expansion coefficient above T_g, α_f, $4.8 \times 10^{-4} K^{-1}$. Both values are physically plausible. But, as before, the simple rheological model of Fig. 4a leads to a modulus which decreases too steeply with temperature. A much better fit to the data is given by the distribution of Fig. 4b, introducing (as before) one new parameter: the standard deviation $\Delta C_1/C_1$ in C_1, and using it in the same way that ΔQ was used earlier.

2.3. The rubbery modulus

Above T_g, the modulus of linear, amorphous polymers often show a plateau at around 1 MPa. This is close to the modulus of weakly cross-linked rubbers and arises, as far as is known, in a similar way. In the rubbery state, the weak intermolecular (Van der Waals) bonds have largely melted. The long chain-like molecules can assume a variety of configurations in response to the thermal vibration which causes a "micro-Brownian" motion of the units of the chain. The most probable configurations are those which maximize the entropy of the system. But there is a constraint; the molecular chains curl and twist around each other; in places they form mechanical entanglements which behave very like chemical cross-links (Fig. 11). When strained, the chains tend to order (by lining up) and the entropy decreases; but the entanglements give the structure a memory, and on unloading it resumes its original shape and the entropy increases again. The rubbery modulus is related to this change in entropy by an equation which is the analog, for entropy-induced elasticity, of Equation 2

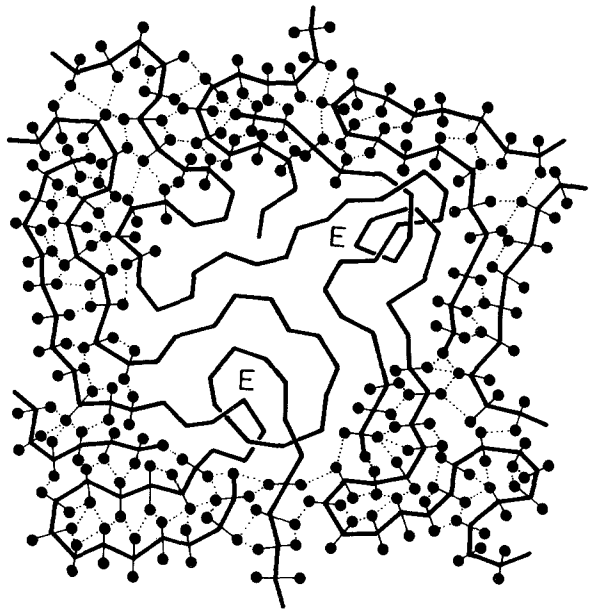

Figure 11 Schematic illustration of a polymer network showing entanglement points (marked "E") which act like chemical cross-links.

$$E = T\frac{d^2S(\varepsilon)}{d\varepsilon^2} \tag{15}$$

where $S(\varepsilon)$ is the entropy per unit volume as a function of tensile strain ε.

Standard texts [7, 9, 17] summarize the calculation of the rubbery modulus from this entropy-dominated model. For small strains the result is

$$E = \frac{3\varrho(T)RT}{\bar{M}_e} \tag{16}$$

where $\varrho(T)$ is the density of the rubbery polymer, R is the gas constant, T the temperature and $\bar{M}_e$ is the average molecular weight between cross-links or (here) entanglement points.

The statistical mechanics of entanglements in linear polymers is, at present, beyond the scope of rubber theorists; $\bar{M}_e$ cannot be calculated and is derived instead from data for E by using Equation 16; values are listed in Table I. This means that the entropy model of rubber elasticity has not, strictly speaking, been verified for linear polymers, although it is difficult to visualize another cause for the rubbery behaviour; and

the values of $\bar{M}_c$ derived from the equation are physically sensible.

At first sight, Equation 16 suggests that the modulus in the rubbery regime should increase with increasing temperature, and for many cross-linked rubbers, it does. But the density decreases with increasing temperature. If the density at some reference temperature (say, T_g) is $\varrho(T_g)$ and the volumetric coefficient of thermal expansion is α_v, then the density at some higher temperature T is

$$\varrho(T) = \frac{\varrho(T_g)}{1 + \alpha_v(T - T_g)} \quad (17)$$

This change in density (which is included in our calculations) cancels, to some extent, the explicit temperature dependence of Equation 16. Further, it is likely that the weaker entanglements unravel as the temperature is increased so that $\bar{M}_e$, too, increases with temperature. The combined influence of this and of thermal expansion leads to the plateau (usually with a slight negative slope) seen in experiments.

2.4. Rubbery and Newtonian viscous flow

At high temperature ($T \gtrsim 1.2T_g$) the Van der Waals bonds melt completely and even the entanglement points slip. This is the regime in which thermoplastics are moulded; the polymer behaves like a viscous liquid. For a given polymer system (such as PMMA) the viscosity, η, depends on the molecular weight, $\bar{M}_w$ and the temperature T.

Two regimes of flow have been identified. Immediately after the rubber plateau, the polymer flows in a way which has the same time–temperature equivalence as that of the visco-elastic regime (Equation 8) implying that it is controlled by free volume. This is generally called "rubbery flow". Then the viscosity is given by

$$\eta = \eta_0 \exp\left[-\frac{C_1(T - T_0)}{C_2 + T - T_0}\right] \quad (18)$$

(where T_0 is the temperature at which $\eta = \eta_0$).

At higher temperaturs and low shear rates, flow follows an Arrhenius law with a narrow spectrum of activation energies, so that, to a good approximation

$$\eta = \eta_0 \exp\left(\frac{Q_m}{RT}\right) \quad (19)$$

The modulus is then calculated from the equations given in the Appendix.

The value of η_0 depends on the molecular weight, $\bar{M}_w$, in one of two ways. Below a critical molecular weight, M_{cr}, the viscosity is proportional to molecular weight so that

$$\eta = \eta_{cr}\frac{\bar{M}_w}{M_{cr}} \quad (20)$$

where η_{cr} is the viscosity of a melt with molecular weight M_{cr}. But above M_{cr}, the dependence changes such that

$$\eta = \eta_{cr}\left(\frac{\bar{M}_w}{M_{cr}}\right)^{3.4} \quad (21)$$

Commercial polymeric systems are in this second regime; and in the range of temperature covered by the diagrams shown in the next section, rubbery flow dominates.

The understanding of this behaviour is still incomplete. Progress in physical modelling has been made by Doi and Edwards [18–21] who extended the work of Rouse [22] and of De Gennes [23] to describe the process of polymer-chain reptation. The polymer chains behave like tangled, flexible strings, each enclosed in a tube made up of the surrounding mass of polymer (Fig. 8). Extension or shear of the polymer requires the diffusive motion of the string in its tube. In the Rouse [22] approach, the Brownian motion is resisted by a Stokes friction; equivalently, compressive or tensile *kinks* form on the chain and diffuse along its length (Fig. 9): the passage of one kink along the entire chain displaces it by the kink-strength, b. If the chains are short and straight, as in Fig. 9, the time required for a kink to diffuse along a chain is simply proportional to the molecular weight. But if the chains are long and tangled, the (stress-biased) random walk, or reptation of a chain in its tube is more complicated. Doi and co-workers [18–20, 24] show that the viscosity should then vary as $\bar{M}_w^3$, in fair agreement with the observations described by Equation 21.

Data for the quantities v_0, $\bar{M}_w$, M_{cr} are listed in Table I.

2.5. Decomposition

If the polymer gets too hot, the thermal energy exceeds the cohesive energy of some part of the molecular chain causing depolymerization or degradation. Some (like PMMA) decompose into monomer units; others (PE, for instance) randomly degrade into many products. It is commercially important that no decomposition takes place during high temperature moulding, so a maximum safe working temperature is specified for each polymer; typically, it is about $1.5T_g$ (Table I). We have truncated the deformation diagrams at this temperature.

3. Data for PMMA and PS

In the last section, we discussed constitutive equations for each of the four main deformation regimes. we now fit data to these equations, extracting values for the parameters (like E_0, α_m, Q_m, ΔQ, T_g, etc.) which best describe them. The final choice of parameters has already been presented in Table I. But the method used to obtain them is an important part of the process for constructing the maps shown later. The data are drawn from many sources, referenced in the text and on the figures and tables.

3.1. Thermal and structural data

Glass temperatures, measured calorimetrically and by dilatometry, are listed in Table II. We have selected

TABLE II Glass transition temperatures (high M_w)

Material	Glass temperature, T_g(K)
PMMA	378 [25], 378 [26], 377 [27], 377 [28], 388 [29], 378 [39], 378 [31]
PS	373 [32], 373 [33], 389 [34], 373 [31]

TABLE III Young's modulus and temperature dependence*

Polymer	Modulus, E_0 (GPa)	α_m
PMMA	8.57†	0.28†
	10.51‡	–
	7.70§	–
PS	6.21¶	0.28¶
	5.80‡	
	6.25§	

*E_0 is Young's modulus extrapolated to 0 K; α_m is the normalized temperature dependence (Equation 3).
†Sinnot [35] extrapolated from 4 K and calculated from G assuming $\nu = 0.33$.
‡Yannas and Luise [3] numerical average from other sources [37] and [36] are included in the PS average.
§Bondi [37].
¶Sinnott [36] extrapolated from 4 K and calculated from G assuming $\nu = 0.33$.

the values shown in Table I as the most reliable. The thermal expansion coefficients (Table I) are from Yannas and Luise [3], Williams *et al.* [6] and Van Krevelen [30]. The molecular weights given in Table I are typical values for commercial PMMA and PS, though, in practice, they vary widely depending on the supplier and the grade.

3.2. The glassy modulus and the secondary relaxations

The modulus at absolute zero, E_0, and its temperature dependence, α_m, were obtained by back-extrapolation of the data of Sinnott [35, 36]. The values obtained in this way for PMMA are close to the average for all the available data; and those for PS are supported by data from Bondi [37], (Table III).

The mean activation energy Q_m for each of the secondary relaxations is found by plotting the log of the time t (or frequency ν) for the centre of the modulus drop (or the damping peak associated with the transition) against $1/T$. It is found (e.g. [38]) that the data follow a simple Arrhenius law so that the plot gives a straight line with slope $-Q_m/2.3R$. For PMMA (Fig. 12a) the β-relaxation has a mean activation of 121 kJ mol^{-1} in agreement with the measurements of Iwayanagi and Hideshima [39, 40] and of Sato *et al.* [41]. The activation energy for the β-relaxation is 13 kJ mol^{-1}. For PS (Fig. 12b) the β-relaxation has a mean activation energy of 132 kJ mol^{-1}. Only two data points ([36, 42]) are available for the δ-relaxation in PS so Q_m was calculated from these directly.

When the relaxations are well separated (as they are for PS) the drop in modulus ΔE associated with each can be measured directly. When this is not so (as for PMMA), ΔE for each transition was adjusted to give the best fit for the overall drop in modulus. Finally the spread of activation energies, $\Delta Q/Q_m$, was chosen by trial and error to match the breadth of the transition. The parameters which fit various groups of data are listed in Table IV and abstracted in Table I. The predictions of the rheological model, using these parameters, are compared with raw data in Figs 13a–c. In practice, the δ-transition in PMMA and the γ-transition in PS have a very small effect on the moduli ($\Delta E < 0.1$ GPa) and they are ignored in constructing the diagrams.

3.3. The glass–rubber transition and the rubbery modulus

The glass–rubber or α-transition, too, is modelled by the rheological model shown in Fig. 4b. The modulus drop ΔE is the difference between the glassy modulus, reduced by the modulus drops associated with the secondary transitions and with thermal expansion (Equation 3), and the rubbery modulus. The mean value of C_1 and its standard deviation were chosen as described earlier. For PMMA, a standard deviation of 0.055 gives a good fit to data (Fig. 14a); for PS, the value 0.08 gives a good fit (Fig. 14b).

The rubbery modulus is related to the molecular weight between entanglements $\bar{M}_e$, by Equation 15. The most recent measurements for commercial polymers are those of Seitz [55] and it is his data that we have used to select $\bar{M}_e$ for PS. But for PMMA a range of values for the rubbery modulus and density have been reported. Results derived from these are listed in Table V; the value we have selected for $\bar{M}_e$ is about half the value given by Seitz. The density $\varrho(T_g)$ at the glass temperature was calculated by extrapolating data for ϱ from the measurement temperature to T_g.

Fig. 15 shows the experimental shift factors, log a_T, for PMMA and PS. Above T_g they are well fitted by

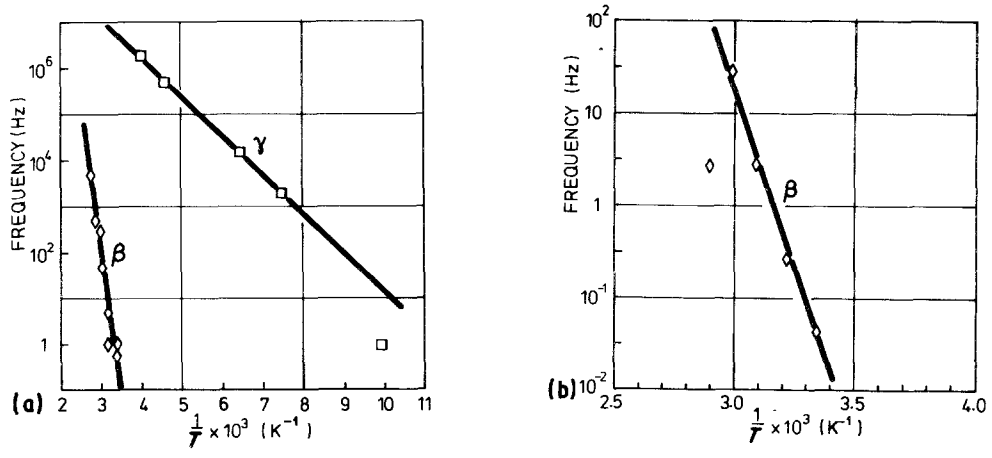

Figure 12 Arrhenius plots of the frequency of damping peak: (a) the β and γ peaks in PMMA; (b) the β peak in PS (after McCrum *et al.* [38]).

TABLE IV Secondary transition data*

Polymer	Transition	Q_m (kJ mol^{-1})	T^* (K)	ΔE (GPA)	ΔQ (kJ mol^{-1})
PMMA	β	75.4 [43] 121.5 [39, 60] 75.4 [44] 125.7 [41] 71.2 [45]	283 [51]	3.55‡	24‡
PMMA	γ	13.0 [46]	100 [71]	1.66‡	2.57§
PMMA	δ	< 20.9 [47]	< 4.2 [35]	< 0.1 [35] < 0.1 [42, 53]	–
PS	β	125.7 [48] 138.3 [49]	300 [52]	0.2‡	55§
PS	γ	33.5 [50]	132 [50]	< 0.07 [34] 0.075 [50]	–
PS	δ	9.4†	36†	1.79 [53] 0.9 [36] > 1.0 [37] > 0.5 [54]	5§

*Q_m is the mean activation energy, T^* the temperature characterizing the damping peak at a frequency of 1 Hz, ΔE the modulus drop associated with the transition and ΔQ the spread in Q required to fit the experimental data.
†Calculated from [53] and [36].
‡Best fit to data this study.
§Estimated value using the method described in the text.

the WLF equation (Equation 8) with values of C_1 and C_2 which are consistent with values of f_g and α_f listed in Table VI. The figures show that at T_g there is a discontinuity in slope of the shift factor. The expansion data given in Table VI suggest that α_f is smaller below T_g, but that it is not zero. We have therefore used the WLF equation below T_g, with a new value of C_2, calculated from the data in Table VI. The final choice of C_1 and C_2 are listed in Table I. The viscosity in the viscoelastic transition has been calculated as described in Section 2, using these parameters in the WLF equation.

3.4. Rubber (glass) – viscous transition and decomposition

Data for viscous flow are summarized in Table VII. The modulus is calculated by using Equations 17 and 18 with the data listed in Table I, including a spread of the constant C_1. Decomposition data are summarized in Table VIII.

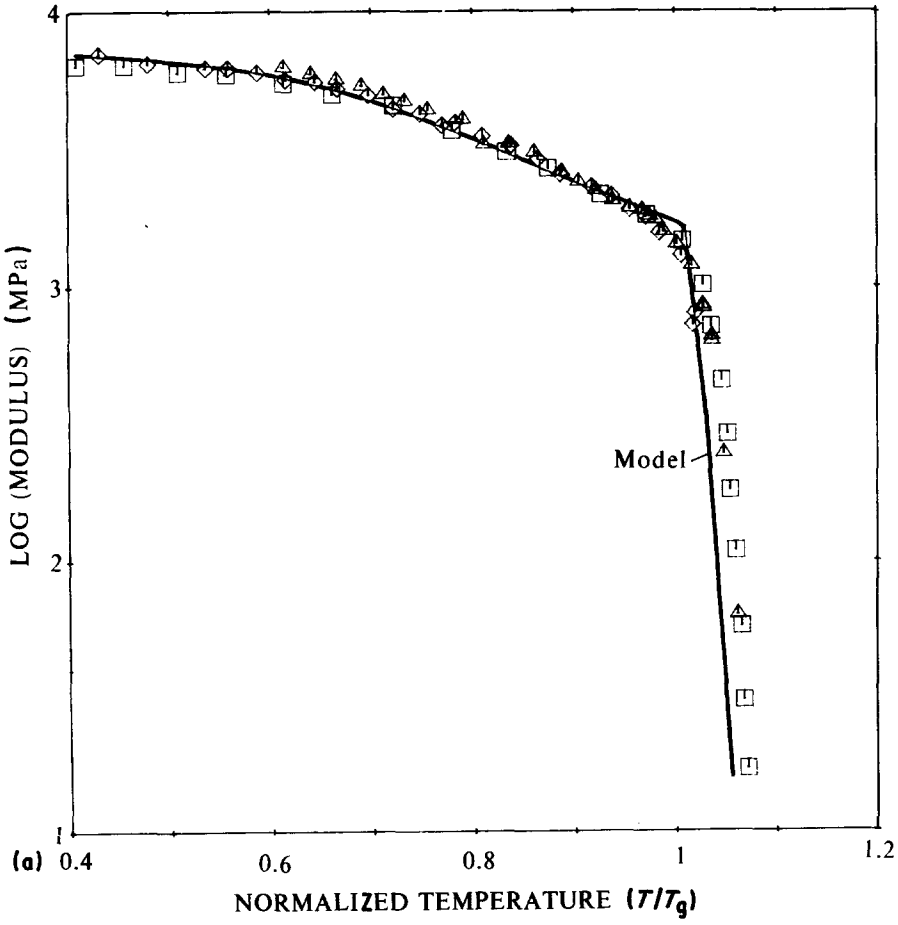

Figure 13 Comparison of data from various sources with the model: (a) PMMA at 1 Hz through T_g, (b) PS at 1 Hz through T_g, (c) PS at 1 Hz at low temperature. The data are taken from references [34, 37, 50, 51, 59].

Figure 13 continued.

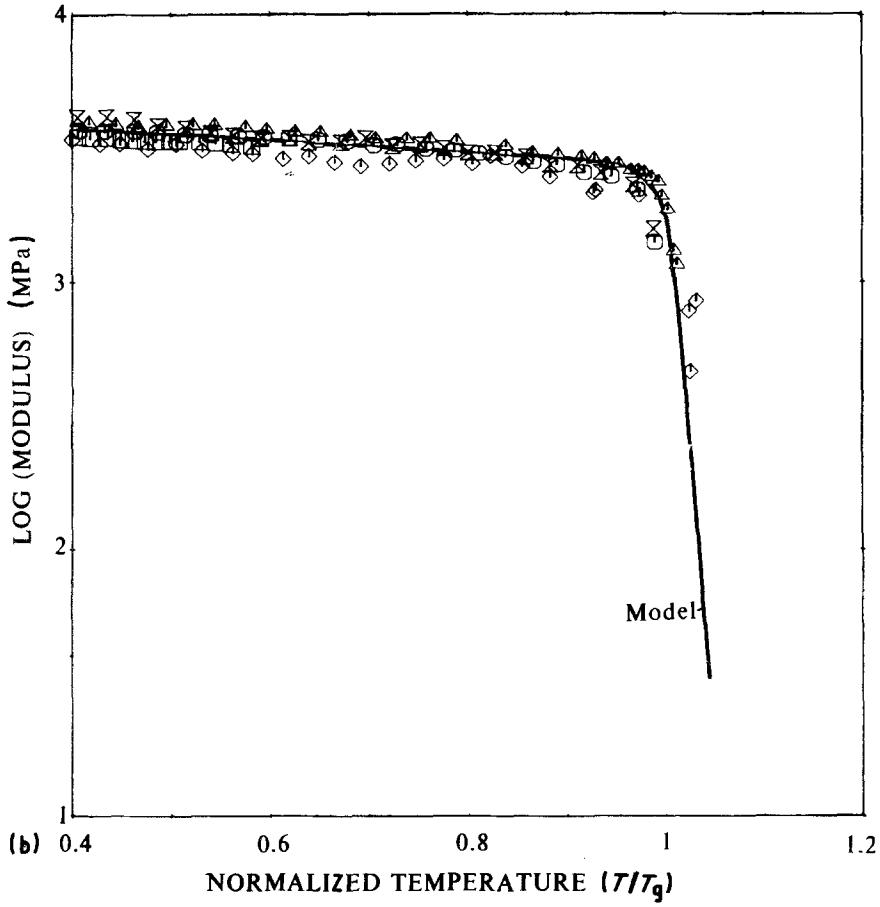

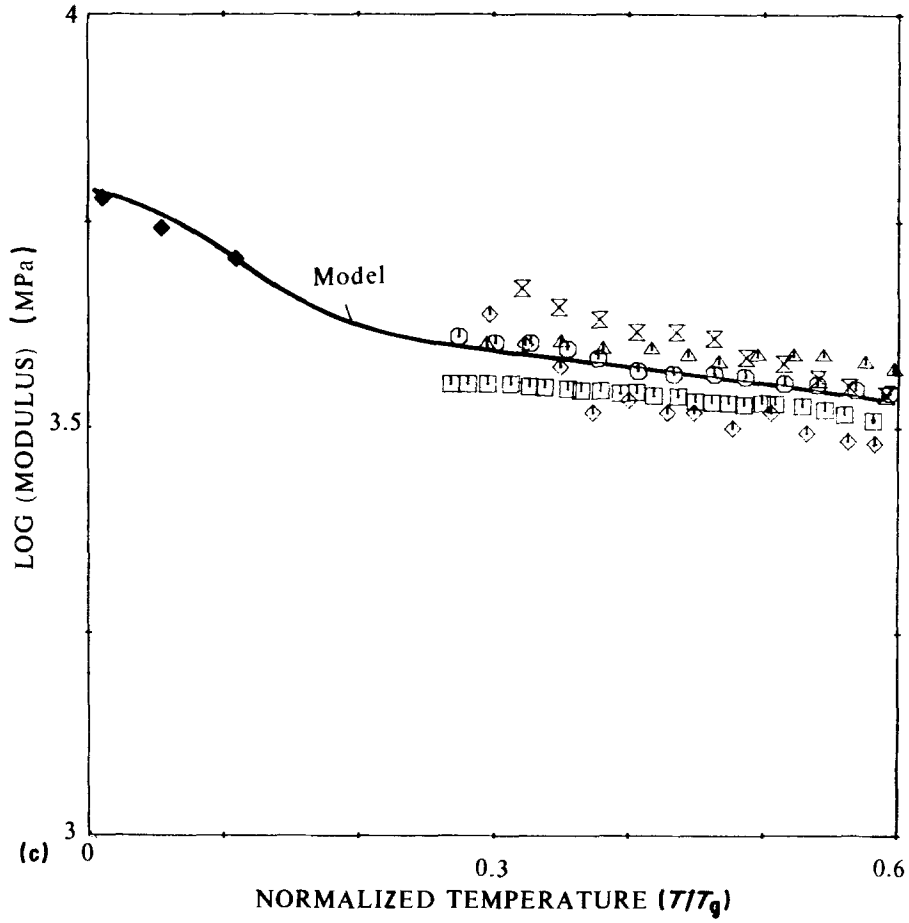

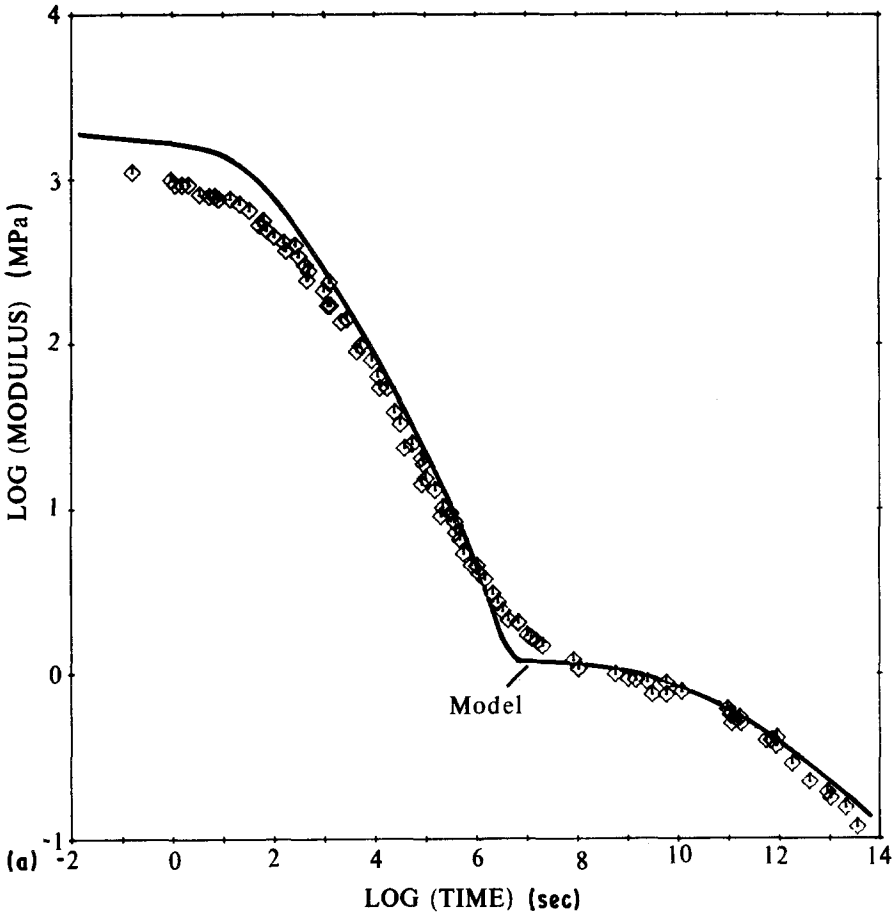

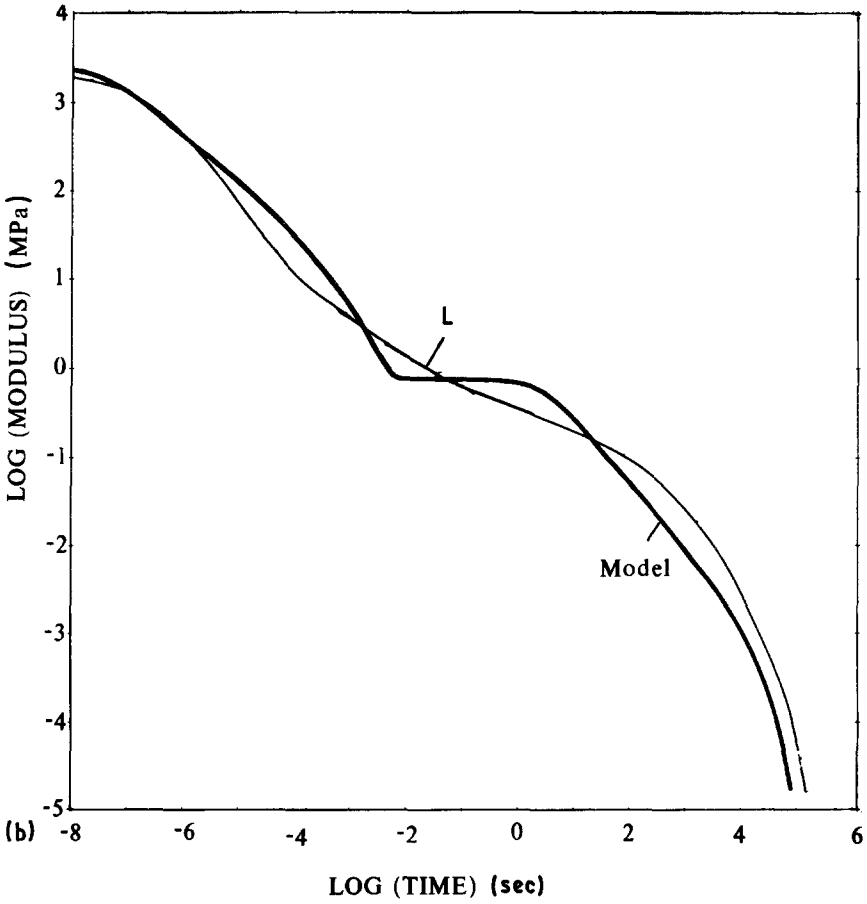

Figure 14 Comparison of stress relaxation data and the predictions of the combined models (a) for PMMA at 373 K, Fujino *et al.* [65], and (b) for PS at 408 K (L) Fujita and Ninomiya [72].

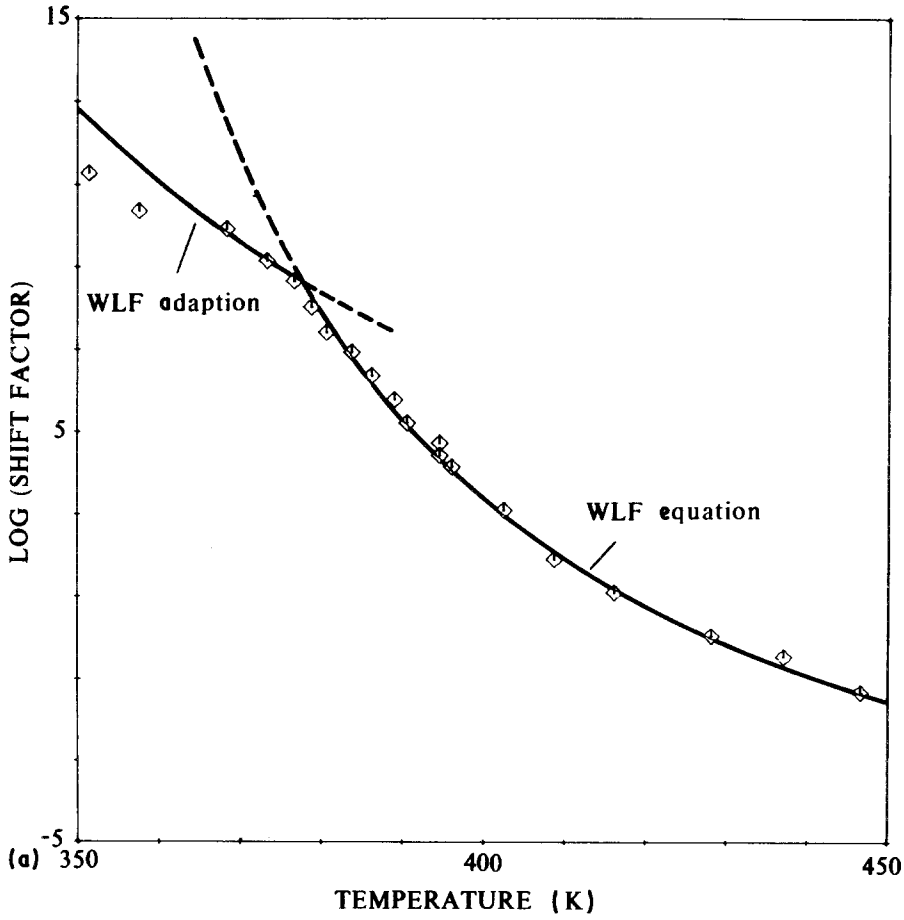

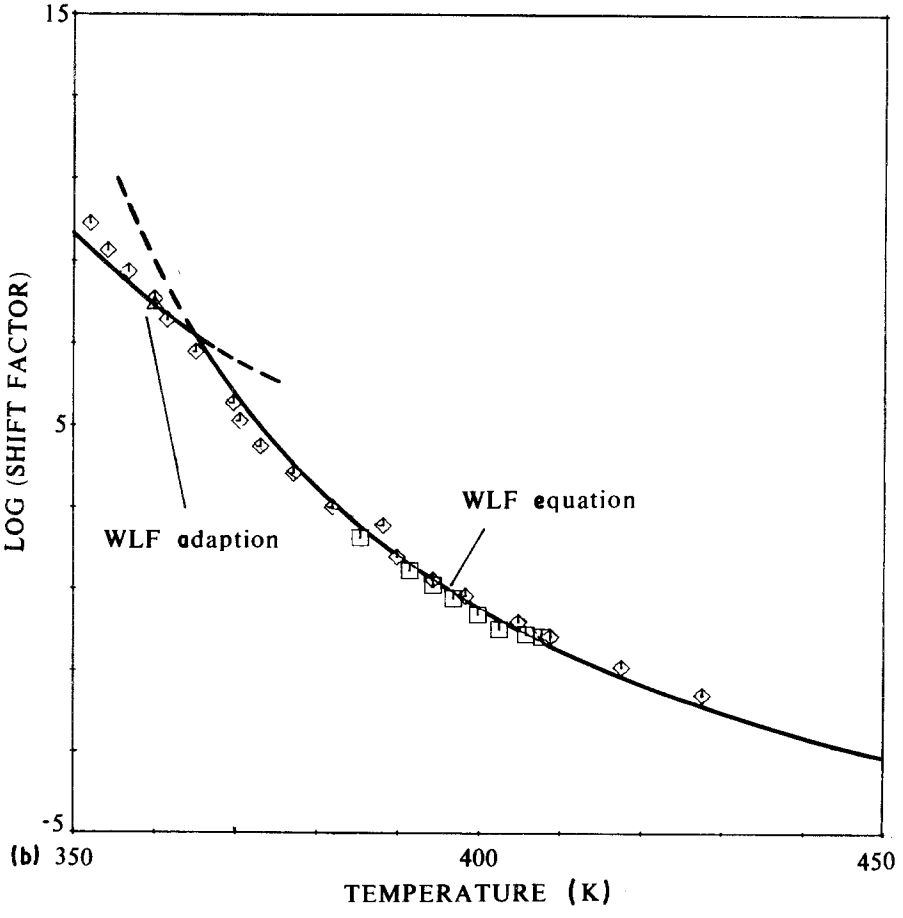

Figure 15 The WLF shift factors calculated using the method of the text, compared with experiments (a) for PMMA, and (b) for PS. (b) (◇) Fujita and Ninomiya [72].

TABLE V Molecular entanglement weight, density and expansion coefficients*

Polymer	$\bar{M}_e$ (kg mol^{-1})	ϱ (10^3 kg m^{-3})	α_g (K^{-1})	α_v (K^{-1})	$\varrho(T_g)$ (10^3 kg m^{-3})
PMMA	9.15 [56] 10.0 [56]	1.188 [28] 1.195† 1.188‡ 1.150§ 1.216¶ 1.19 [61]	2.7×10^{-4} [30]	6.2×10^{-4} [30] 6.6×10^{-4} [30]	1.16**
PS	19.1 [55] 18.1 [57]	1.04–1.065 [62] 1.05¶ 1.057† 1.052–1.065 [63]	1.8 [30] 2.8 [30]	4.5 [30] 7.1 [30]	1.03**

* M_e is the molecular weight between entanglements, calculated from Equation 16, ϱ is the density at the temperature listed in the reference, α_g is the bulk expansion coefficient below T_g and α_v is that above T_g; $\varrho(T_g)$ is the mean density extrapolated to T_g.
† Kolb and Izard [58] at 273 K.
‡ Gall and McCrum [59] at 298 K.
§ Rogers and Mandelkern [26] at T_g.
¶ Fujino *et al.* [60] at 298 K.
**Calculated from data presented.

4. Modulus–mechanism diagrams

4.1. Construction and features of the diagrams

The previous sections have described the mechanisms which determine the modulus of linear amorphous polymers between absolute zero and the decomposition temperature. We now ask: over what range of time and temperature is a given mechanism dominant? And when do the changes of mechanism appear? For each mechanism, the constitutive equation takes the form

$$E = f(t \text{ or } v,\ T, \text{ material properties}) \quad (22)$$

where t is the loading time (or v is the frequency) and T is the absolute temperature. The dominant mechanism, for a given T and t, is the one which leads to the lowest value of E; and mechanism changes take place where two mechanisms lead to the same modulus*.

Figs 16 to 19 show deformation mechanism diagrams for PMMA and PS, constructed from the constitutive equations of Section 2, using the parameters of Table I, always selecting the one that leads to the lowest modulus. Details are given in the Appendix. Figs 16 and 17 show the dynamic modulus of PMMA over the full ranges of temperature and frequency that can be realized in practice. In Fig. 16 the axes are E and T; the contours are lines of constant fequency. The four regions are roughly distinguished by the range of modulus which characterizes them, as suggested by Tobolsky [68], though strictly it is a field of values of E, T and v, not merely of E, which characterizes a mechanism. In Fig. 17 the axes are E and v (plotted inversely to make the diagram comparable with diagrams which have time as abscissa: see Gilbert [64]). Here too, the four mechanism-regimes are distinguished by a range of values of E. Figs 18 and 19 show similar diagrams for PS.

4.2. Influence of polymer chemistry and molecular weight

It seems probable that these diagrams for PMMA and PS are broadly typical of those for linear amorphous polymers. By normalizing the temperature scale by T_g, the lowest-order effects of differing polymer chemistry are removed.

At any more detailed level, of course, there are effects of polymer chemistry and molecular weight. The α, β, γ and δ transitions are determined by the nature of the side-groups, since these influence the packing of molecules in the amorphous state. (The experiments of Fujino *et al.* [65] on co-polymers of PMA and PMMA, for example, show that the larger the side-groups, the more difficult it is to pack the chains, and the broader is the glass–rubber transition.) The extent of the rubbery regime, too, depends on the molecular weight of the polymer. Reducing the molecular weight shifts the contours in the viscous flow

TABLE VI Free volume data*

Material	α_v at T_g (K^{-1})	α_g at T_g (K^{-1})	α_0 at T_g (K^{-1})	$\alpha_f(T < T_g)$	$\alpha_f(T > T_g)$
PMMA	6.25×10^{-4}†	2.69×10^{-4} ‡	9.4×10^{-5}§	1.75×10^{-4}§	5.31×10^{-4}¶
PS	6.12×10^{-4}†	2.27×10^{-4}‡	5.8×10^{-5}§	1.69×10^{-4}§	5.4×10^{-4}¶

* α_v and α_g are the bulk expansion coefficient above and below T_g, α_0 is the expansion coefficient for the occupied volume (Fig. 9), α_f is the difference. C_1 and C_2 in Table I are calculated from these data using $C_1 = B/2.303 f_g$ and $C_2 = f_g/d_f$, with $B = 1$ (Williams *et al.* [63]) and $f_g = 0.025$ (Doolittle [14, 15]).
† Van Krevelen ([30], Table 4.10).
‡ Average values in [30].
§ Calculated by Gilbert [64].
¶ Williams *et al.* [6].

* The response of the rheological model for the relaxations is evaluated numerically, summing the Gaussian distribution of activation energies over $3\Delta Q$ on either side of Q.

TABLE VII Viscous flow*

Polymer	v_0 (N sec m^{-2})
PMMA	2×10^{-2}†
PS	1.4×10^{-5}‡

*v_0 is the pre-exponential viscosity in Equation 18.
†Chosen to fit the data of Fujino *et al.* [65].
‡Chosen to fit the data of Fujita and Nimoniya [72].

TABLE VIII Depolymerization temperatures

Polymer	T_d	T_d/T_d
PMMA	543*	1.44
PS	543†	1.46

*Dosser [66].
†Shell Plastics [67].

regimes to the left, and reduces the extent of the rubbery plateau or removes it altogether. McLoughlin and Tobolsky [69], for instance, find that PMMA with a molecular weight of 36 kg mol^{-1} shows a pronounced rubbery plateau, while that with a molecular weight of 0.15 kg mol^{-1} shows none. Other studies of the extent of the rubbery regime can be understood in these terms (Vinogradov *et al.* [70]). And the viscosity of the melt regime, too, depends on molecular weight (Van Krevelen, [30]), though the differences scale, broadly, as T_g.

We expect, therefore that linear amorphous will be described by diagrams like those of Figs 16 to 19, with small differences caused by molecular weight and architecture.

5. Summary and conclusions

Maps can be constructed which summarize the time and temperature dependent modulus of amorphous polymers, $E(t, T)$, for a wide range of temperatures and times, under various loading conditions. Several separate mechanisms are involved: bond stretching, constrained molecular movement and larger scale molecular sliding, rubbery behaviour constrained by entanglements and true viscous flow. Each mechanism can be modelled (though with differing levels of physical realism) to give constitutive equations which describe how the modulus $E(t, T)$ depends on temperature, time or frequency of loading, and on material parameters which characterize the chemistry and molecular architecture of the polymer. We have assembled material parameters for PMMA and for PS and used them, with the constitutive equations, to construct the maps shown as Figs 16 to 19.

It is probable that the maps shown here are broadly typical of linear amorphous polymers (though maps for others can readily be constructed using the same method). The same approach can be adapted to describe amorphous thermosets and rubbers, and, with further changes, to commercially significant semicrystalline polymers such as nylon and PE.

The maps shown here describe small-strain behaviour. The next step, we believe, is to develop a parallel approach for large strain deformation which is capable of including cold drawing, shear banding, twinning and crazing.

Appendix: computation of the deformation diagrams

The modulus E is calculated as a function of temperature T and loading frequency v ("dynamic loading") or time ("stress relaxation"). At the highest temperatures, E is determined by viscous flow. The modulus, which we will term E_{vR} is then determined by a dashpot describing the faster of the two flow mechanisms (Equations 18 and 19) in series with a spring describing the rubber-modulus E_R. Further decrease in temperature introduces the glass–rubber transition. Let the increase in modulus associated with this

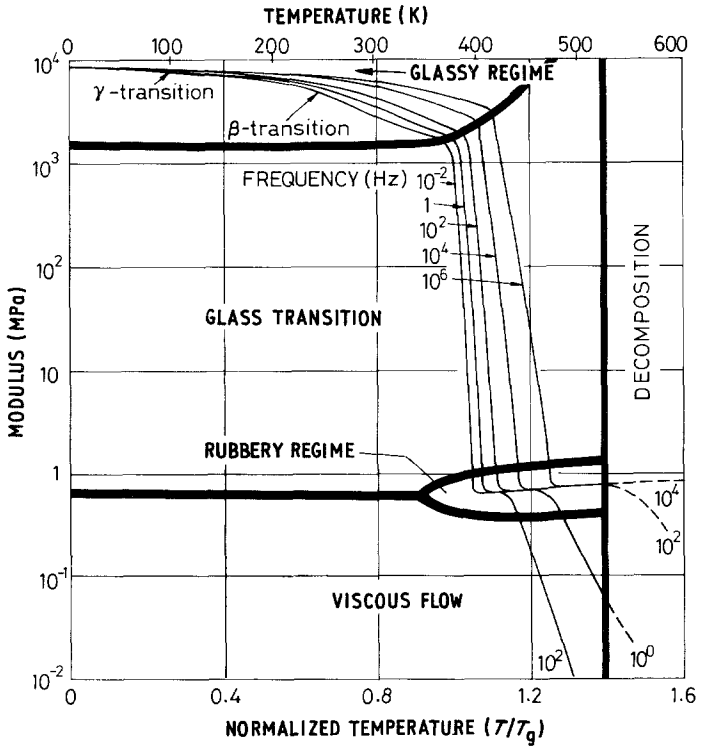

Figure 16 A deformation diagram for PMMA under dynamic loading conditions, with E and T/T_g as axes.

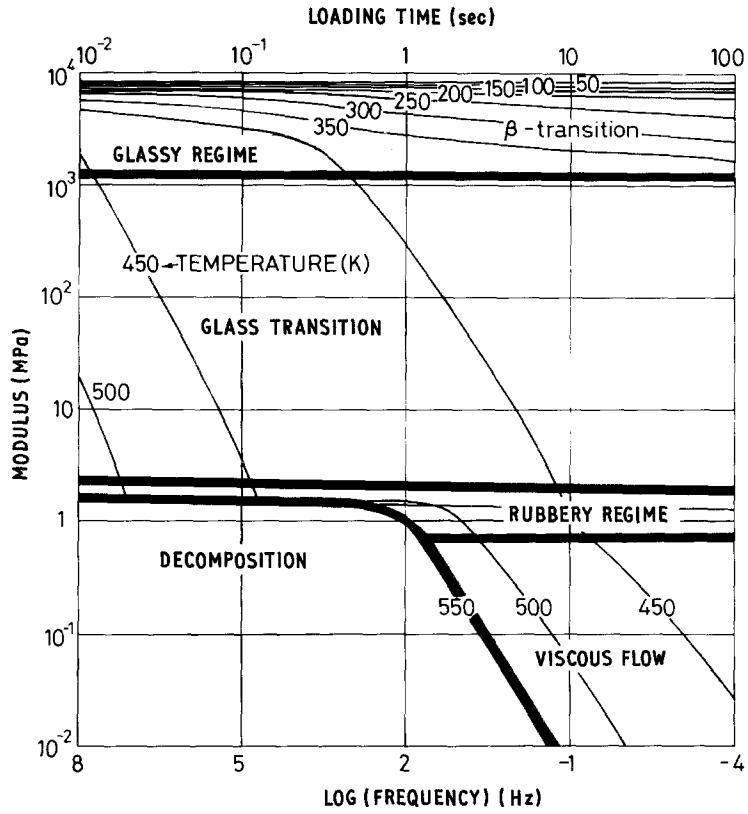

Figure 17 A deformation diagram for PMMA under dynamic loading conditions, with E and frequency ν as axes.

transition be ΔE_α (defined below). Further drop in temperature freezes out the β, γ and δ relaxations; let the increase in modulus caused by these be ΔE_β, ΔE_γ and ΔE_δ. Then the modulus, at temperature T and frequency ν is

$$E(T, \nu) = E_{\nu R} + \Delta E_\alpha + \Delta E_\beta + \Delta E_\gamma + \Delta E_\delta \tag{A1}$$

To proceed further, we require expressions for the individual ΔE terms. Conside the β relaxation as an example. It is described by the array of n Maxwell elements shown in Fig. 4b. For a single element

$$\dot{\varepsilon} = \frac{\dot{\sigma}}{E} + \frac{\sigma}{\eta} \tag{A2}$$

Then for the parallel array of Fig. 4b, the following constitutive equations hold. If the modulus associated with the ith element is δE_i and its viscosity is $\delta\eta_i$ (Fig. 4), then for constant strain

$$\Delta E_\beta = \sum_{i=1}^{n} \delta E_i \exp\left(-\frac{\delta E_i t}{\delta \eta_i}\right) \tag{A3}$$

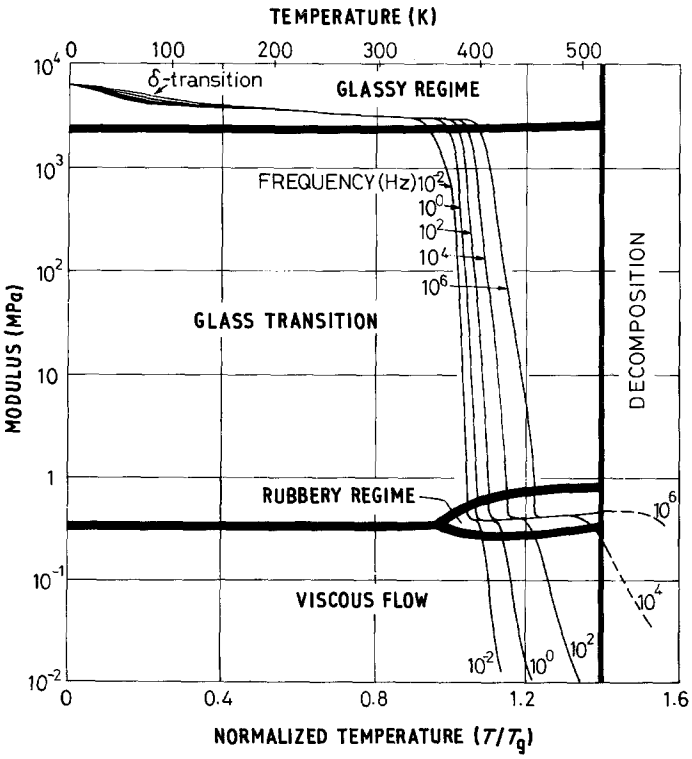

Figure 18 A deformation diagram for PS under dynamic loading conditions, with E and T/T_g as axes.

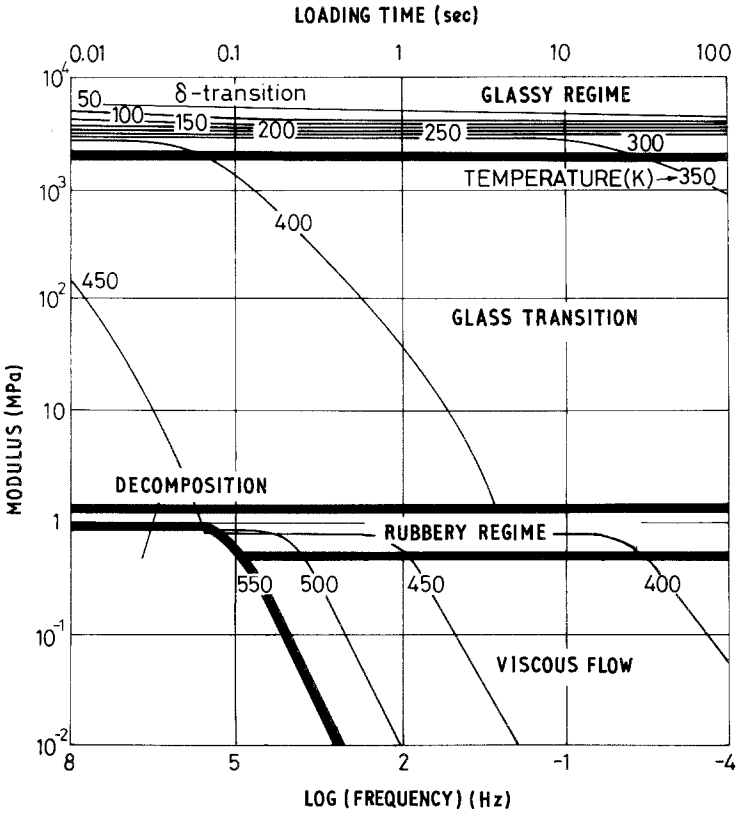

Figure 19 A deformation diagram for PS under dynamic loading conditions with E and frequency ν as axes.

for constant strain rate

$$\Delta E_\beta = \sum_{i=1}^{n} \frac{\delta\eta_i}{t}\left[1 - \exp\left(-\frac{\delta E_i t}{\delta\eta_i}\right)\right] \quad \text{(A4)}$$

and for dynamic loading (so that $\varepsilon = \varepsilon_0 \sin \nu t$)

$$\Delta E_\beta = \sum_{i=1}^{n}\left[\frac{\delta E_i}{1 + \left(\frac{\delta E_i}{\nu\delta\eta_i}\right)^2}\right] \quad \text{(A5)}$$

where

$$\delta E_i = \Delta E_\beta^0 f(Q)\delta Q \quad \text{(A6)}$$

$$\delta\eta_i = \delta_{0\beta} \exp\left(\frac{Q_i}{RT}\right) f(Q)\delta Q. \quad \text{(A7)}$$

and ΔE_β^0 is the total modulus change associated with the β transition. Similar expressions are used for the δ and γ transitions; the α or glass transition only differs in the expression used for ξ: it is (from Equation 14)

$$\delta\eta_i = \eta_{0\alpha} \exp \frac{C_{1i}(T - T_g)}{C_2 + T - T_g} f(Q)\delta Q \quad \text{(A8)}$$

The rubbery flow regime is treated in a similar way.

An important quantity in each summation is the standard deviation of the activation energy. It determines, through Equation 5, the breadth of each transition. The standard deviations of Q (for the β, γ and δ transitions) and of C_1 (for the α and rubbery flow regimes) are listed in Table I as the "fractional spread" in each quantity: $\Delta Q/Q_m$ and $\Delta C_1/C_1$. Values of ΔE were determined at each temperature and frequency by evaluating Equation A3, A4 or A5, summing the Gaussian distribution over $3\Delta Q$ (or $3\Delta C_1$) on either side of Q or C_1.

Acknowledgements

We wish to thank Dr L. M. Brown, Dr D. J. Brown, Mr P. A. Smith and Dr A. M. Donald for many very helpful discussions. We wish to acknowledge the support of the US Army European Research Office through a research contract, and the SERC through the award of a studentship.

References

1. P. B. BOWDEN, *Polymer* **9** (1968) 449.
2. I. V. YANNAS, in "Deformation in Glassy Polymers – Molecular Interpretation", Proceedings of the IUPAC Symp., Rio de Janeiro (Elsevier, Amsterdam 1974) p. 1.
3. I. V. YANNAS and R. R. LUISE, *J. Macromol. Sci. Phys.* **B21** (1982) 443.
4. P. J. FLORY, in "Statistical Mechanics of Chain Molecules" (Interscience, New York, 1969).
5. L. M. BROWN, in Proceedings of the 3rd Riso Conference, edited by E. Lilholt and R. Talreja (Riso National Laboratory, Denmark, 1982) p. 1.
6. M. L. WILLIAMS, R. L. LANDEL and J. D. FERRY, *J. Amer. Chem. Soc.* **77** (1955) 3701.
7. I. M. WARD, "Mechanical Properties of Polymers" (Wiley, New York, 1971).
8. R. F. C. ARRIDGE, "Mechanics of Polymers" (Oxford University Press, Oxford, 1975).
9. R. J. YOUNG, "Introduction to Polymers" (Chapman and Hall, London, 1981).
10. M. H. COHEN and D. TURNBULL, *J. Chem. Phys.* **31** (1959) 1164.
11. R. N. HAWARD (ed), in "The Physics of Glassy Solids" (Applied Science, London, 1973) p. 1.
12. F. BUECHE, *J. Chem. Phys.* **22** (1953) 603.
13. A. S. ARGON and L. T. SHI, *Phil. Mag.* **46** (1982) 275.
14. A. K. DOOLITTLE, *J. Appl. Phys.* **22** (1951) 1471.
15. *Idem, ibid.* **23** (1952) 236.
16. J. D. FERRY, "Viscoelastic Properties of Polymers" (Wiley, New York, 1961) Ch. 11.
17. L. R. G. TRELOAR, "The Physics of Rubber Elasticity", Clarendon Press, Oxford, 1958).
18. M. DOI and S. F. EDWARDS, *J. Chem. Soc., Faraday Trans.* **74** (1978) 1789.
19. *Idem, ibid.* **74** (1978) 1802.
20. *Idem, ibid.* **75** (1979) 38.
21. *Idem, ibid.* **74** (1978) 1818.

22. P. E. ROUSE Jr, *J. Chem. Phys.* **21** (1953) 1272.
23. P. G. DE GENNES, *ibid.* **55** (1971) 572.
24. M. DOI, *J. Polym. Sci. Polym. Phys. Ed.* **21** (1983) 667.
25. S. LOSHAEK, *J. Polym. Sci.* **15** (1955) 391.
26. S. S. ROGERS and L. MANDELKERN, *J. Phys. Chem.* **61** (1957) 945.
27. J. C. WITTMANN and A. J. KOVACS, *J. Polym. Sci.* **C16** (1969) 4443.
28. T. G. FOX, *J. Amer. Chem. Soc.* **80** (1958) 1768.
29. G. C. BERRY and T. G. FOX, *Adv. Polym. Sci.* **5** (1967) 261.
30. D. W. VAN KREVELEN, "Properties of Polymers" (Elsevier, Amsterdam, 1976).
31. T. G. FOX, S. GRATCH and S. LOSHAEK, in "Rheology: Theory and Applications" edited by F. R. Eirich (Academic Press, New York, 1956) Ch. 12.
32. T. G. FOX and P. J. FLORY, *J. Appl. Phys.* **21** (1950) 581.
33. D. J. PLAZEK, *J. Phys. Chem.* **69** (1965) 3480.
34. K. VON SCHMEIDER and K. WOLF, *Kolloid-Z.* **134** (1953) 149.
35. K. M. SINNOTT, *J. Polym. Sci.* **35** (1959) 272.
36. *Idem, Soc. Plast. Eng. Trans.* **2** (1962) 63.
37. A. BONDI, "Physical Properties of Molecules, Crystals, Liquids and Glasses" (Wiley, New York, 1969) p. 394.
38. N. G. McCRUM, B. E. READ and G. WILLIAMS, "Anelastic and Dielectric Effects in Polymer Solids" (Wiley, London, 1967).
39. S. IWAYANAGI and T. HIDEHSIMA, *J. Phys. Soc. (Jpn.)* **8** (1953) 365.
40. *Idem, ibid.* **8** (1953) 368.
41. K. SATO, *ibid.* **9** (1954) 413.
42. J. M. CRISSMAN, A. E. WOODWARD and J. A. SAUER, *J. Polym. Sci.* **A2** (1965) 2693.
43. K. DEUTSCH, E. A. W. HOFF and W. REDDISH, *ibid.* **13** (1954) 565.
44. J. HEIJBOER, *Kolloid-Z.* **148** (1956) 36.
45. N. G. MCcRUM and E. L. MORRIS, *Proc. R. Soc.* **A281** (1964) 258.
46. K. M. SINNOTT, *J. Polym. Sci.* **42** (1960) 3.
47. F. A. JOHNSON and J. C. RADON, *Eng. Fract. Mech.* **4** (1972) 555.
48. O. YANO and Y. WADA, *J. Polym. Sci.* **A2** (1971) 669.
49. T. M. CONNOR, *ibid.* **A2** (1970) 191.
50. K. M. ILLERS and E. JENCKEL, *ibid.* **41** (1959) 528.
51. J. HEIJBOER, in "Physics of Non-Crystalline Solids" (North Holland, Amsterdam, 1965) 231.
52. K. M. ILLERS and E. JENCKEL, *Rheol. Acta.* **1** (1958) 322.
53. J. M. CHRISSMAN, A. E. WOODWARD and J. A. SAUER, *J. Polym. Sci.* **A1** (1964) 5075.
54. H. HENDUS, *Ergeb. Exakt. Naturw.* **31** (1959) 220.
55. J. T. SEITZ, 50th Golden Jubilee of the Rheology Society, Boston, Mass. (1979).
56. T. MASUDA, K. KITAGAWA and S. ONOGI, *Polym. J. (Jpn.)* **1** (1970) 418.
57. S. ONOGI, T. MASUDA and K. KITAGAWA, *Macromols* **3** (1970) 109.
58. M. J. KOLB and E. F. IZARD, *J. Appl. Phys.* **20** (1949) 564.
59. W. G. GALL and N. G. McCRUM, *J. Polym. Sci.* **50** (1961) 489.
60. K. FUJINO, K. SENSHU and H. KAWAI, *Rept. Prog. Polym. Phys. (Jpn.)* **5** (1982) 107.
61. T. E. BRADY and G. S. Y. YEH, *J. Appl. Phys.* **42** (1971) 4622.
62. G. NATTA, *J. Polym. Sci.* **16** (1955) 143.
63. J. T. WILLIAMS and K. J. CLEEREMAN, in "Styrene, Its Polymers, Co-polymers and Derivatives" edited by R. H. Boundy and R. F. Boyer (Reinhold, New York, 1952) Ch. 10.
64. D. G. GILBERT, PhD thesis, Cambridge University (1985).
65. K. FUJINO, *et. al. J. Colloid Sci.* **16** (1961) 262.
66. J. M. DOSSER, private communication (1983).
67. Shell Plastics, Technical Bulletin PS2.1 "Shell Polystyrene Safety Data and Information" (1983).
68. A. V. TOBOLSKY, "Properties and Structure of Polymers" (Wiley, New York, 1960).
69. J. R. McLOUGHLIN and A. V. TOBOLSKY, *J. Colloid. Sci.* 7 (1952) 555.
70. G. V. VINOGRADOV, *et al. J. Polym. Sci.* **A2** (1971) 1153.
71. J. G. POWLES and P. MANSFIELD, *Polymer* **3** (1962) 336.
72. H. FUJITA and K. NINOMIYA, *J. Polym. Sci.* **14** (1957) 233.

Received 25 October
and accepted 20 December 1985